Influence of shock absorber damping rates on the fatigue of anti-roll bars of a commercial vehicle

Arthur Larocca*
and Mina Youssef

Volvo Group Canada, Inc.,
1000 Industriel Blvd.,
Saint-Eustache, QC J7R 5A5, Canada
Email: arthur.larocca@outlook.com
Email: mina.youssef.1@ulaval.ca
*Corresponding author

Anne Gadbois

University of Sherbrooke,
2500 University Blvd.,
Sherbrooke, QC J1K 2R1, Canada
Email: anne.gadbois@usherbrooke.ca

Dragos Zamfir

Volvo Group Canada, Inc.,
1000 Industriel Blvd.,
Saint-Eustache, QC J7R 5A5, Canada
Email: dragos.zamfir.1@ens.etsmtl.ca

Pablo Kubo

Volvo Trucks Brazil,
Rua João Dembinski, 371,
casa 40, Curitiba, 81270-330, Brazil
Email: pyykubo@hotmail.com

Abstract: Within the framework of an integrated product development, the main objective of this study is to assess the influence of shock absorber damping rates on the fatigue of anti-roll bars of a commercial vehicle. In this regard, force and displacement data have been collected in a durability test track with an instrumented bus on curb weight (CW) and gross axle weight rating (GAWR). Based on the theory of fatigue damage accumulation, the durability of each anti-roll bar of a bus (front and rear suspension) was assessed for three different shock absorber damping rates. Statistical significance between different shock absorbers has been identified for both bars on both loading conditions. The results pointed out that, in some cases, a softer damper could reduce by almost half the fatigue life of an anti-roll bar when compared to the same bar with stiffer dampers.

Keywords: anti-roll bar; stabiliser bar; shock absorber; damper; damping rate; damping coefficient; fatigue; damage; commercial vehicle; concurrent engineering; integrated product development.

Reference to this paper should be made as follows: Larocca, A., Youssef, M., Gadbois, A., Zamfir, D. and Kubo, P. (2020) 'Influence of shock absorber damping rates on the fatigue of anti-roll bars of a commercial vehicle', *Int. J. Heavy Vehicle Systems*, Vol. 27, Nos. 1/2, pp.180–201.

Biographical notes: Arthur Larocca received his Bachelor of Science in Mechanical Engineering. He is Verification & Validation Supervisor at Volvo Group Canada.

Mina Youssef received his Master's degree in Mechanical Engineering. He is Test Engineer at Volvo Group Canada.

Anne Gadbois is a Mechanical Engineer student at Université de Sherbrooke, in Canada.

Dragos Zamfir received his Bachelor of Science in Mechanical Engineering. He is Test Engineer at Volvo Group Canada.

Pablo Kubo received his PhD in Mechanical and Civil Engineering. He is Durability and Ride & Handling Feature Leader at Volvo Trucks Brazil.

1 Introduction

In a continually changing market, many companies of the automotive industry have to improve their product development process to stay competitive. One consideration is to enhance the product development cycle by optimising product design and increasing its efficiency during the initial design phase (Su, 2014; Tan and Vonderembse, 2006). In this concern, organisations are moving from the traditional design-build-test cycle to a combined and synchronised task approach, mainly driven by front-load analysis, simulation and testing (Milburn, 2004). Although the broad context of concurrent engineering has been explored by many authors (Ebrahimi, 2011; Hambali et al., 2009; Haug, 2012; Sapuan et al., 2006), from the perspective of the validation of new products it is important to assess how different concepts can impact the loads applied on a given system. This will help calculations and test schedules to be well defined on an early design stage.

Within this context, the parameters and configurations of a vehicle's suspension have an important role. By converting the kinetic energy of suspension movement into heat energy (Rana et al., 2014), shock absorbers are selected and tuned to improve comfort, ride and handling characteristics of a vehicle (Dixon, 2007; Neal et al., 2015; Soone et al., 2005). Anti-roll bars, also known as stabiliser bars, are used in vehicle suspensions in order to reduce the body roll displacement and roll angle during single wheel lifting and cornering manoeuvre (Hijawi and Czaja, 2004; Noraishikin et al., 2012).

While some studies have analysed the loads and fatigue of anti-roll bars (Ribeiro and Silveira, 2013; Senapathi et al., 2009; Topaç et al., 2011) and others have addressed the influence of shock absorbers on the vertical load (Kubo et al., 2015) and on the ride and handling (Hegazy and Sandu, 2009; Kokane et al., 2015; Rakheja et al., 1999), there is a lack of studies on the dynamic interaction between dampers and stabiliser bars from a durability standpoint.

To address this research gap, the main objective of this study is to assess the influence of shock absorber damping rates on the fatigue of anti-roll bars. Given the relevance of ride comfort (Eriksson and Friberg, 2000; Zhu et al., 2014) and reliability (Eriksson and Friberg, 2001; Sert and Pinar, 2017) for the bus transit services, this work will focus on the suspension system of a city bus.

Using experimental data, this study aims to contribute to the literature by providing more insight on the verification and validations phases within product development in the automotive industry. Since it associates concepts of vehicle dynamics with the theory and calculation of fatigue prediction, a brief literature review is presented in Sections 1.1 and 1.2. While Section 1.1 connects the vibration theory of a half-car model with the experimental test performed, Section 1.2 presents the concepts and equations used for the fatigue analyses of the tested anti-roll bars.

1.1 Vibration theory of a half-car model

To examine the problematic from a theoretical standpoint, a half car vibrating model is presented in Figure 1. The model proposed by Jazar (2008) includes the road excitations y_1 and y_2, wheels hop x_1 and x_2, body bounce x, body roll φ and mass moment of inertia I_x. The suspension model is symmetrical (b is the distance between each tyre and the centre of gravity (C) of the sprung mass); it considers the shock absorbers damping coefficient (c) and also the stiffness of the tyre (k_t), the air spring (k_a) and the anti-roll bar (k_{ARB}).

Figure 1 Half-car model

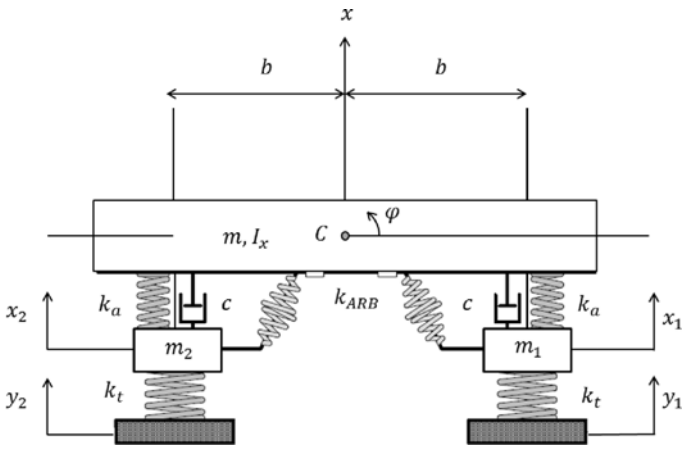

Source: Adapted from Jazar (2008, p.860)

Jazar (2008) proves that Newton's equation of motion can be converted to the Lagrange form:

$$\frac{d}{d_t}\left(\frac{\partial K}{\partial \dot{q}_r}\right)-\left(\frac{\partial K}{\partial q_r}\right)=F_r \tag{1}$$

where K is the kinetic energy of n degree of freedom system, q_r, $r=1,2,3,\ldots,n$ are the coordinates of the system and F_r is the force combined to q_r.

From Figure 1, the kinetic and potential energies of the system are:

$$K=\frac{1}{2}m\dot{x}^2+\frac{1}{2}m_1\dot{x}_1^{\,2}+\frac{1}{2}m_2\dot{x}_2^{\,2}+\frac{1}{2}I_x\dot{\varphi}^2 \tag{2}$$

$$\begin{aligned}V=&\frac{1}{2}k_t\left(x_1-y_1\right)^2+\frac{1}{2}k_t\left(x_2-y_2\right)^2+\frac{1}{2}k_{ARB}\varphi^2\\&+\frac{1}{2}k_a\left(x-x_1+b\varphi\right)^2+\frac{1}{2}k_a\left(x-x_2+b\varphi\right)\end{aligned} \tag{3}$$

and the dissipation function:

$$D=\frac{1}{2}c\left(\dot{x}-\dot{x}_1+b\dot{\varphi}\right)^2+\frac{1}{2}c\left(\dot{x}-\dot{x}_2-b\dot{\varphi}\right) \tag{4}$$

Applying the Lagrange Method,

$$\frac{d}{d_t}\left(\frac{\partial K}{\partial \dot{q}_r}\right)-\left(\frac{\partial K}{\partial q_r}\right)+\left(\frac{\partial D}{\partial \dot{q}_r}\right)+\left(\frac{\partial V}{\partial q_r}\right)=f_r \qquad r=1,2,3,\ldots \tag{5}$$

The re-arranged equations of motion for the half car vibrating model of a vehicle in a matrix form are as follow:

$$F=\lceil m\rceil\ddot{x}+[c]\dot{x}+[k]x \tag{6}$$

$$\mathbf{F}=\begin{vmatrix}0\\0\\y_1k_t\\y_2k_t\end{vmatrix} \tag{7}$$

$$\mathbf{m}=\begin{vmatrix}m & & & \\ & I_x & & \\ & & m_1 & \\ & & & m_2\end{vmatrix} \tag{8}$$

$$\mathbf{c}=\begin{vmatrix}2c & 0 & -c & -c\\ 0 & 2cb^2 & -cb & cb\\ -c & -cb & c & 0\\ -c & cb & 0 & c\end{vmatrix} \tag{9}$$

$$\mathbf{k} = \begin{vmatrix} 2k_a & 0 & -k_a & -k_a \\ 0 & 2k_a b^2 & -k_a b & k_a b \\ k_a & -k_a b & k_a + k_t & 0 \\ -k_a & -k_a b & 0 & k_a + k_t \end{vmatrix} \tag{10}$$

$$\mathbf{x} = \begin{vmatrix} x \\ \varphi \\ x_1 \\ x_2 \end{vmatrix} \tag{11}$$

In the half car model presented above, the road excitations y_1 and y_2 have to be different to introduce a roll angle φ on the vehicle. The roll angle generates a difference between the body bounce x and the wheels x_1 and x_2, producing a proportional torque on the anti-roll bar $(M_{ARB} = -k_{ARB}\varphi)$.

Based on the equations of motion above, a primary objective of this work is to evaluate how the change of the damping coefficients (c) of the shock absorbers would affect the transferred forces to the anti-roll bar – what would reflect in its fatigue endurance.

Hassaan (2014) examined the relative displacement between sprung and unsprang mass of a car model at different speeds for different damping coefficients. The Author found that at a same speed, this relative displacement decreases with the increase of the damping coefficient. Based on that, the primary hypothesis of this work is that a higher damping coefficient would reduce the roll angle and, consequently, the forces applied on both extremities of the stabiliser bar.

However, given model uncertainties and theoretical assumptions, an experimental test with a real vehicle is required to draw reliable conclusions regarding the impacts on the durability of the components. For example, while the damping coefficients (c) are generally considered as constant values in the literature (McNaull et al., 2010; Zhang et al., 2019), in reality they are in function of the shock absorber's velocity and operation (compression or rebound) (Kubo et al., 2015). Hence, this work uses the term 'damping rate' to differentiate the dampers settings. For instance, a shock absorber with a higher damping rate is expected to present a higher damping coefficient at a specific velocity and operation when compared to a damper with a lower damping rate on the same conditions.

1.2 Fatigue damage accumulation theory

As structures and mechanical components are regularly subjected to oscillating loads and fatigue is one of the major causes in component failures, fatigue life prediction has become a relevant subject (Liou et al., 1999).

Through a stress-life curve, it is possible to determine the number of cycles for failure in a given signal with constant load. Given the fact that only few applications have such behaviour (constant load), Dowling (2012) presents the following equation:

$$\frac{N_1}{N_{f1}} + \frac{N_2}{N_{f2}} + \frac{N_3}{N_{f3}} + \ldots = \sum \frac{N_j}{N_{fj}} = 1 \tag{12}$$

where N_j is the number of cycles for each constant load and N_{fj} is the number of cycles (failure) from stress-life curve, for each constant load.

Basically, it states that a component will fail when the sum of the ratio between the number of cycles, for each segment, and the number of cycles from stress-life curves, is equal to 1 (Figure 2). Moreover, the damage, represented by those ratios, occurs and accumulates only when the stress is higher than the fatigue limit (Zhu et al., 2011).

Figure 2 Damage accumulation principle

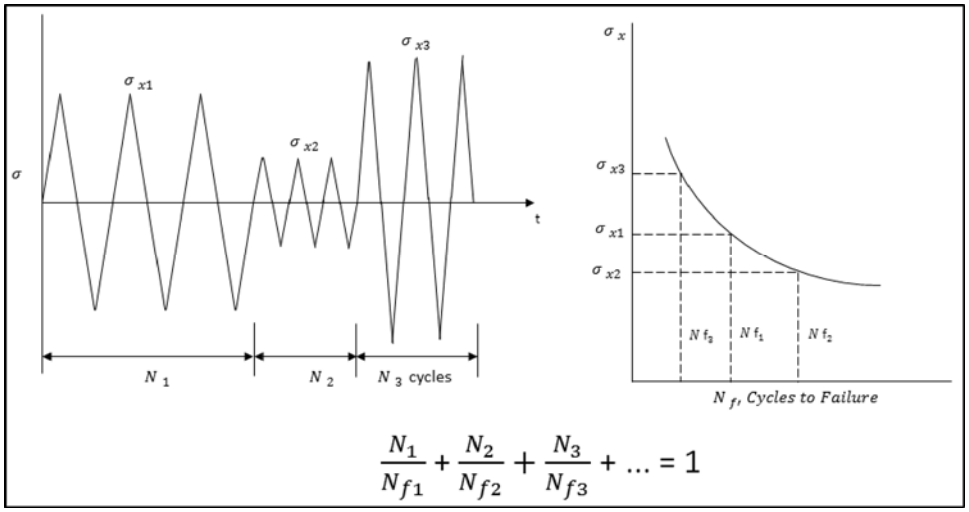

Source: Adapted from Dowling (2012, p.450)

Using the concepts of damage accumulation from Miner (1945) and the theory of rainflow cycle counting by Endo and Matsushi (1968), the concept of absolute fatigue damage can be stated as following:

$$\sigma_a = \frac{(\sigma_{\max} - \sigma_{\min})}{2} \tag{13}$$

where: σ_a is the average amplitude from each rainflow cycle ($\sigma_{\max}$ and $\sigma_{\min}$), $\sigma_{\max}$ is the max amplitude (peak) of each rainflow cycle and $\sigma_{\min}$ is the min amplitude (valley) of each rainflow cycle.

$$N_{fj} = \frac{1}{2}\left(\frac{\sqrt{\sigma_{\max}.\sigma_a}}{\sigma'_f}\right)^{\frac{1}{b}} \tag{14}$$

where N_{fj} is the number of cycles (failure) from stress-life curve, for each constant load, σ'_f is the theoretical loading that indicates failure with zero cycle (material property) and b is the stress-life curve slope (material property).

$$\text{absolute damage} = \sum \frac{N_j}{N_{fj}} \tag{15}$$

Lastly, Dowling (2012) defines the concept of fatigue relative damage as the ratio between the absolute damage of two different load histories:

$$\text{relative damage} = \frac{\text{absolute damage}_1}{\text{absolute damage}_2} \tag{16}$$

While the fatigue analyses performed in this work are detailed in the methodology section, the results will be expressed in terms of absolute and relative damage.

2 Methodology

Based on real data collected from an instrumented bus and on a statistical analysis of significance, the durability of each anti-roll bar of a commercial vehicle (front and rear suspension) was assessed for three different shock absorbers' damping rates.

The test vehicle chosen for the test was a 40 feet transit bus with front and rear dependent solid axle suspension systems. The front anti-roll bar was attached to the bus frame and connected to two link rods (one on each side) which were connected to the front axle beam. The rear anti-roll bar was mounted onto the rear axle and attached to two link rods connected to the frame. Figure 3 illustrates the kinematics of the tested system, where the action-reaction force pair (F) is transmitted through the link rods at both ends. The mounting points (on the axle or on the frame) are represented by the two bushings of the anti-roll bar.

Figure 3 Illustration of the forces applied on the anti-roll bars

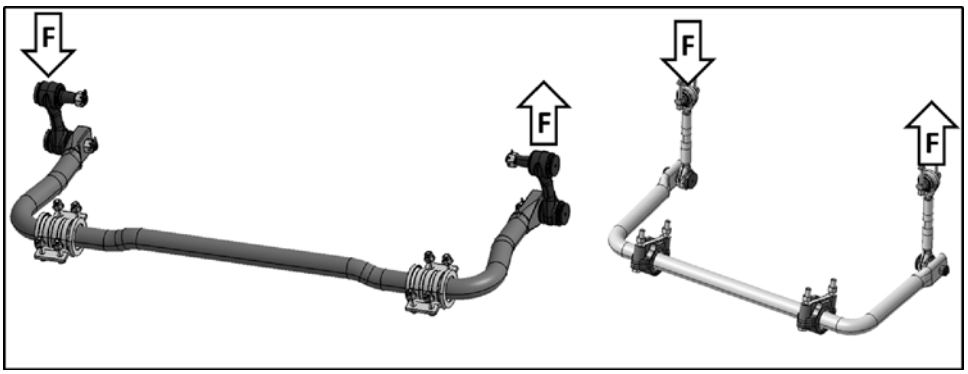

The following subsections cover an overview on the test track, bus instrumentation, shock absorbers, and fatigue and data analyses.

2.1 Test track and manoeuvres

The test has been carried out in a private test track located in Canada. As illustrated in Figure 4, the track consists of seven different stress inducing elements that mimic the type of events expected to be encountered during the service of a bus. The bus speed on the durability elements of the track follows a specific speed profile, such as: 20 mph (32.2 km/h) on the random chuck holes, chatter bumps and high crown intersection;

10 mph (16.1 km/h) on the staggered bumps, frame twist and the end turnarounds; 8 mph (12.9 km/h) on railroad crossing; and 5 mph (8 km/h) on the 4″ Chuck Hole.

Figure 4 Durability element profiles of durability test track

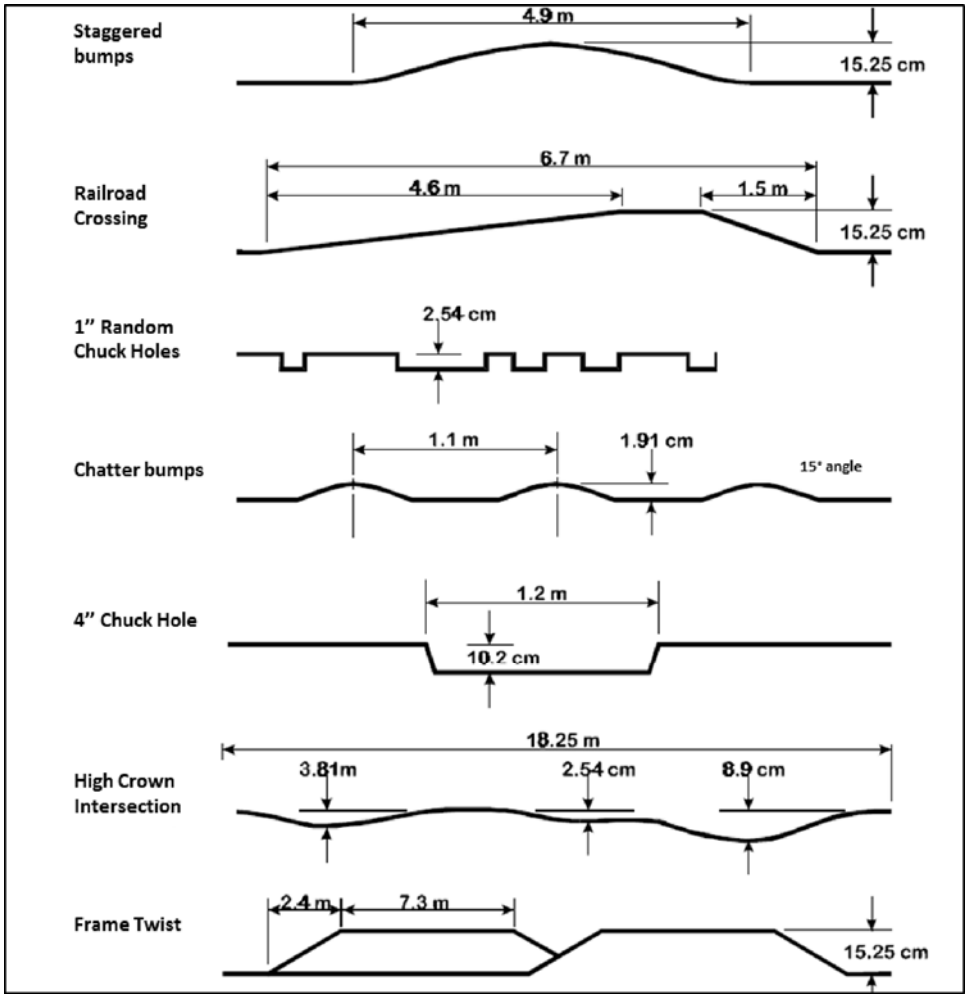

Source: Adapted from Klinikowski et al. (1998, p.4)

For each set of shock absorbers (see Section 2.3), the bus has been tested in its curb weight (approx. 13 tons) and gross axle weight rating (GAWR) (approx. 20 tons) configurations. The data have been acquired for 40 laps on the durability track: 20 laps on clockwise and 20 laps on counter clockwise direction.

2.2 Instrumentation

To measure the forces applied on the anti-roll bars, each of the four links rods (two on the front and two on the rear – Figure 5) was instrumented with strain gauges (350 ohms) in a full Wheatstone bridge arrangement.

Figure 5 Instrumented link rods

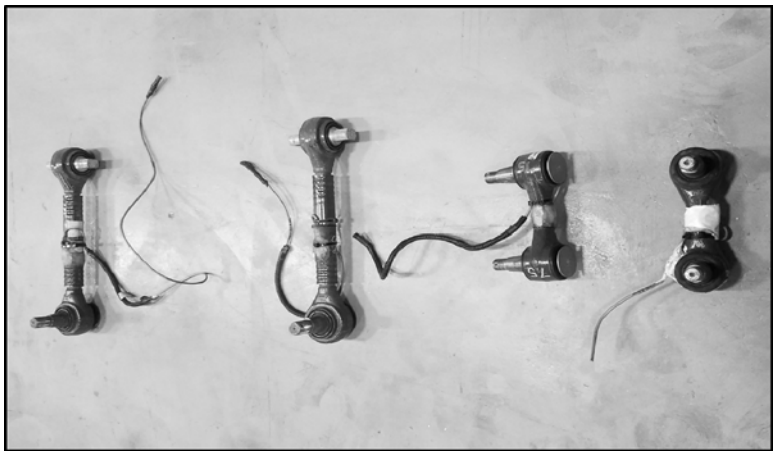

Prior to installing the rods on the bus, they were calibrated for force in a bench test (with a hydraulic actuator and a load cell). Figure 6 presents the obtained calibration curves for each of the link rods, which correlates the strain gauges readings (in mV/V) to the applied force in the bench (in kN).

Figure 6 Calibration curves of the anti-roll bars link rods

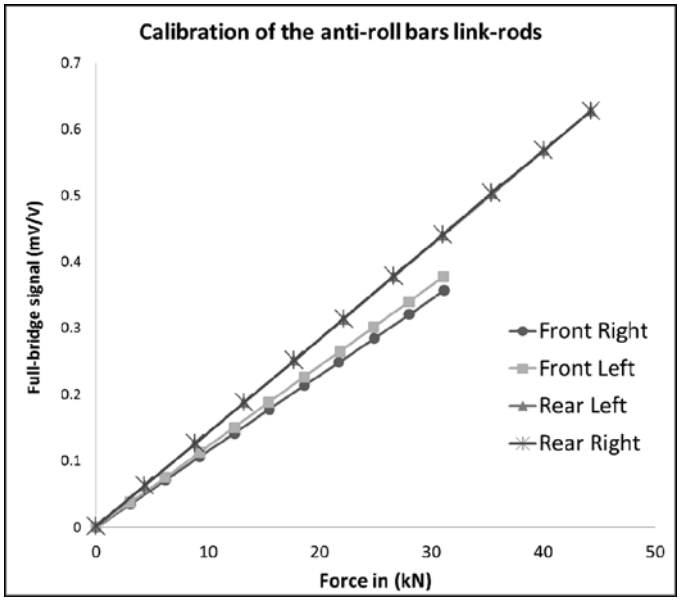

After the calibration, the link rods were assembled in the test bus and were used as dynamic load cells.

Besides the force on the link rods, the displacements of the shock absorbers were also measured during the test. In this regard, string potentiometers (Celesco SP2-50 – full stroke of 1270 mm) were installed on each one of the four shock absorbers, as shown in Figure 7. Differentiating the shocks' displacement with respect to time was useful during

post-processing in order to evaluate the dampers velocity in the different testing configurations.

Two Krypton modules (6xSTG – with six universal differential voltage and bridge inputs) from Dewesoft were used for the data acquisition. The Figure 8 summarises the complete instrumentation and measurement system used in this work.

Figure 7 String potentiometer (Celesco SP2-50) installation on the shock-absorber (see online version for colours)

Figure 8 The complete instrumentation and measurement process

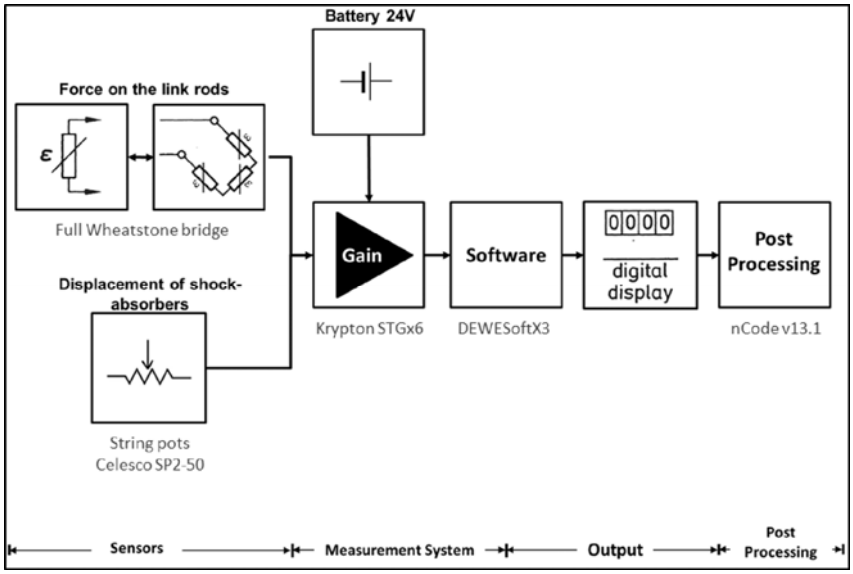

2.3 Shock absorbers

Three different sets of shock absorbers were tested on both front and rear suspension. Each set comprised four shock absorbers, two identical dampers on the front suspension and other two identical on the rear suspension. They were identified according to their damping rates, as below:

1 Soft dampers

2 Intermediate dampers

3 Stiff dampers.

Figures 9 and 10 present the damping forces according to the velocity for the three sets of shock absorbers for the front and the rear suspension, respectively.

Figure 9 Damping forces of front suspension's shock absorbers

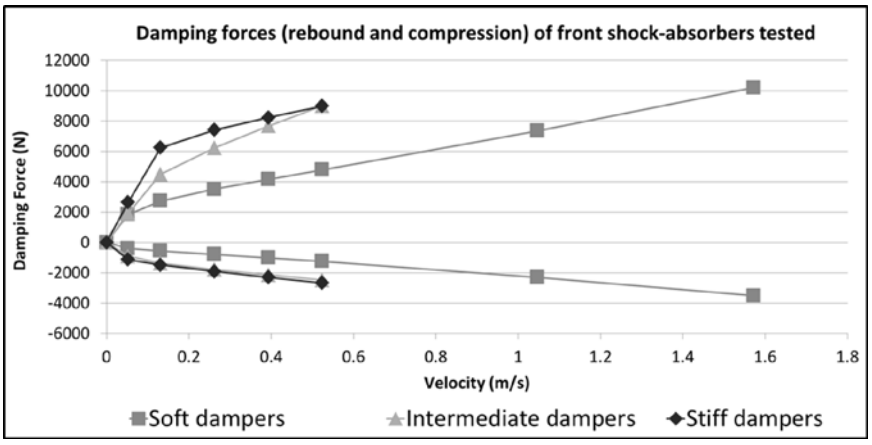

Figure 10 Damping forces of rear suspension's shock absorbers

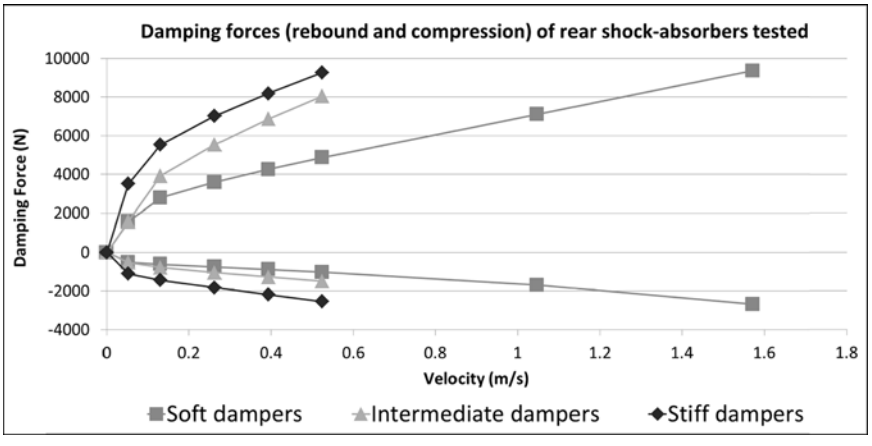

As can be noted and as discussed in Section 2.1, the shock absorbers do not present constant damping coefficients. For this reason, the term 'damping rate' is used to

distinguish the different dampers tested. The stiff dampers are expected to have a higher damping coefficient at a certain velocity and operation (rebound/compression) when compared to the intermediate and soft dampers at the same conditions. The same logic is valid when comparing the intermediate and soft sets.

2.4 Fatigue damage analyses

Finite element (FE) models of the front and rear bars were used in nCode DesignLife™ 13.1, for a SN (Stress-Life) CAE fatigue analysis. With Goodman as the mean stress correction method and absolute max principal criteria, quench and tempered steel 42CrMoS4 (as rolled) was selected as the component material for this analysis. The synthetic fatigue curve of the defined material is presented in Figure 11.

Figure 11 Stress-life curve used for quench and tempered steel – 42CrMoS$_4$ (see online version for colours)

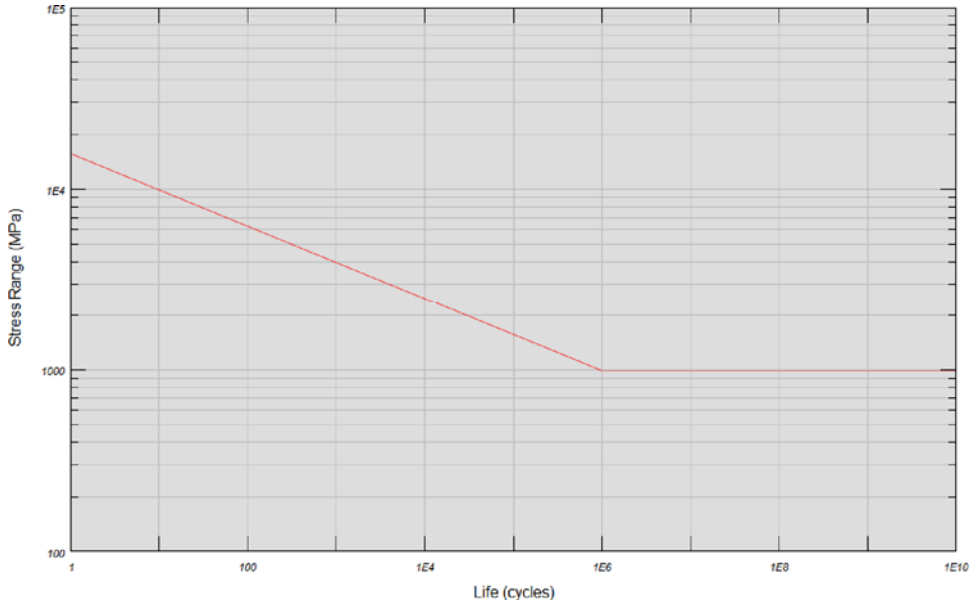

For each bar, damper and bus weight, the fatigue analyses were performed for eight equivalent load cases (forces measured as described in Sections 2.1 and 2.2):

- Load case 1: Force from left link rod, laps 1–10 on clockwise direction.
- Load case 2: Force from left link rod, laps 11–20 on clockwise direction.
- Load case 3: Force from right link rod, laps 1–10 on clockwise direction.
- Load case 4: Force from right link rod, laps 11–20 on clockwise direction.
- Load case 5: Force from left link rod, laps 1–10 on counterclockwise direction.
- Load case 6: Force from left link rod, laps 11–20 on counterclockwise direction.

- Load case 7: Force from right link rod, laps 1–10 on counterclockwise direction.
- Load case 8: Force from right link rod, laps 11–20 on counterclockwise direction.

Theorically, given the track and suspension symmetricity, these load cases would yield identical results for the damage accumulation. Pratically, given experimental uncertainty (mainly random errors), they do not. As such, each load case result was considered as an observation on each of the independent treatments (shock absorber settings).

With two bars, three shock absorbers, two vehicle weights and eight load cases, a total of 96 fatigue analyses were performed. Despite the fact that the outputs from each analysis were a contour plot and a table of absolute damage accumulation on each node of the numeric model, the results and discussions in this work will be based on the maximum fatigue damage value observed for each test configuration.

2.5 Data analyses

Data were assessed for differences between the three shock absorbers settings (independent treatments) using a one-way analysis of variance (ANOVA). Significance was set a priori at $p < 0.05$ and the data from the test in curb weight and GAWR were analysed separately. With statistical significance observed, a post-hoc Tukey's HSD (Honest Significant Differences) test was used to examine specific contrasts (also with significance level equal to 0.05) between each one of the three pairs (number of treatments = 3). As eight load cases were used for each analysis, the error term has 21 degrees of freedom.

As detailed by Abdi and Williams (2010), a statistical significance will be observed when the absolute value of the difference between two given means (from two different groups) is higher than the value of the HSD (Q critical):

$$\left|M_{a+} - M_{a'+}\right| > \text{HSD} = q_{A,} \propto \sqrt{\frac{1}{2} MS_{S(A)} \left(\frac{1}{S_a} + \frac{1}{S_{a'}} \right)} \tag{17}$$

where $\left|M_{a+} - M_{a'+}\right|$ is the absolute difference between two given means (Q statistic), S_a is the error source (obtained through previous ANOVA) and $MS_{S(A)}$ is the mean square of error. The value from $q_{A,} \propto$ can be obtained from Table 1, presented by Harter (1960).

Table 1 Critical values of q for studentised range distribution $\alpha = 0.05$

	No. of treatments			
df error term	*2*	*3*	*4*	*5*
18	2.971	3.609	3.997	4.277
19	2.960	3.593	3.977	4.253
20	2.950	3.578	3.958	4.232
24	2.919	3.532	3.901	4.166
30	2.888	3.486	3.845	4.102
40	2.858	3.442	3.791	4.039

Source: Harter (1960)

3 Results and discussion

Figures 12 and 13 present two output examples of the contour plot of damage accumulation in the FE models of front and rear anti-roll bars, respectively.

Figure 12 SN fatigue analysis of front anti-roll bar: intermediate dampers – curb weight – load case 1 (see online version for colours)

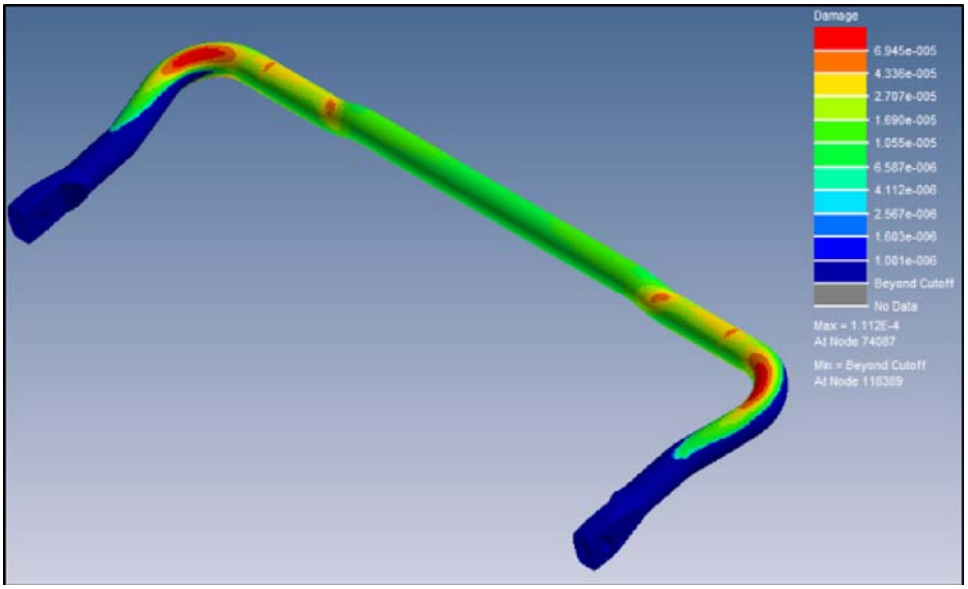

Figure 13 SN fatigue analysis of rear anti-roll bar: soft dampers – GAWR – load case 4 (see online version for colours)

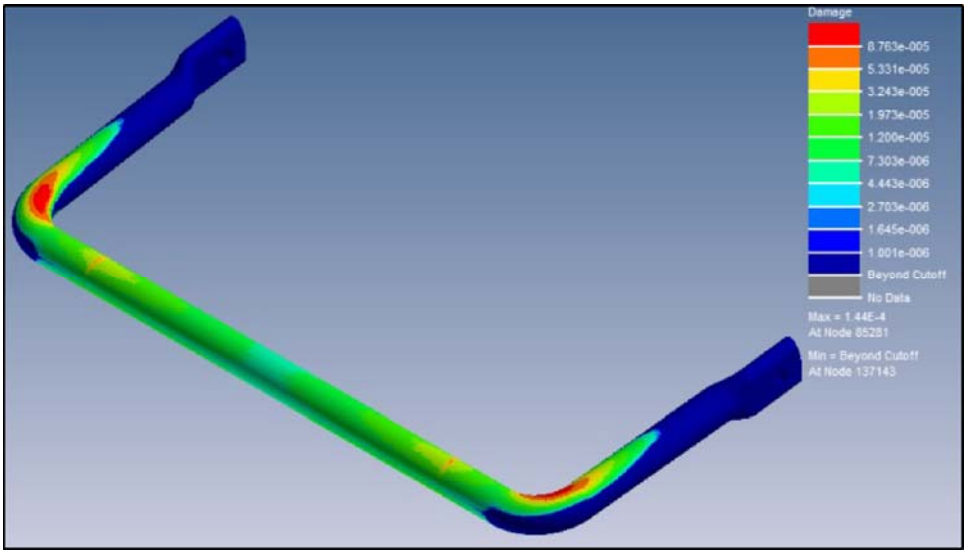

As can be noted, both bars showed a similar hotspot for damage accumulation: on their main bend. Althougth the different test configurations and load cases imposed different damage accumulations, the visual gradient of damage distribution has not changed on the components.

3.1 Front anti-roll bar results

Table 2 presents the maximum absolute fatigue damage values observed on each tested configuration for the front anti-roll bar.

Table 2 Maximum absolute fatigue damage values on the front anti-roll bar

		Absolute fatigue damage		
Bus weight	*Load case*	*Soft dampers setting*	*Intermediate dampers setting*	*Stiff dampers setting*
CW	1	1.250E-04	1.110E-04	8.496E-05
	2	1.230E-04	1.120E-04	9.151E-05
	3	1.490E-04	1.410E-04	9.214E-05
	4	1.580E-04	1.400E-04	9.350E-05
	5	1.268E-04	1.120E-04	7.420E-05
	6	1.320E-04	1.160E-04	7.570E-05
	7	1.540E-04	1.360E-04	7.600E-05
	8	1.450E-04	1.460E-04	7.600E-05
GAWR	1	1.650E-04	1.390E-04	1.060E-04
	2	1.620E-04	1.380E-04	1.030E-04
	3	1.980E-04	1.660E-04	1.440E-04
	4	1.960E-04	1.630E-04	1.280E-04
	5	1.800E-04	1.390E-04	1.080E-04
	6	1.670E-04	1.310E-04	1.090E-04
	7	2.130E-04	1.640E-04	1.420E-04
	8	1.970E-04	1.540E-04	1.350E-04

A comparison of the results is illustrated in Figure 14, which presents a relative fatigue damage analysis of the averaged results from the eight load cases. The results of the intermediate dampers are set as the baseline (100%), while the results from the soft and stiff dampers settings are presented as a percentage of it.

To examine for statistical significance, an ANOVA was carried out for each bus weight (CW and GAWR). As these analyses suggested that the treatments were significantly different, the Tables 3 and 4 present the results of the Tukey HSD test for both configurations (in order to examine specific contrasts between the pairs).

As presented in these tables, significant differences have been observed between all analysed pairs, except for the results between the soft and intermediate dampers settings on curb weight.

Figure 14 Relative fatigue damage analysis of front anti-roll bar – soft and stiff dampers as a percentage of intermediate dampers setting

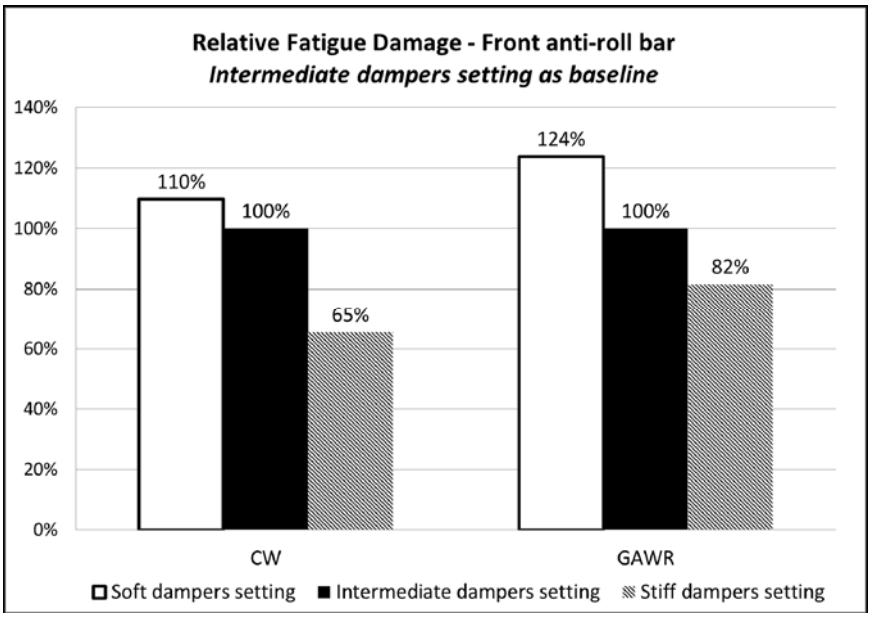

Table 3 Tukey's HSD test – front anti-roll bar on curb weight

Treatments pair	*Tukey HSD Q statistic*	*Tukey HSD Q critical*	*Tukey HSD inference*
Soft *vs.* Intermediate	2.7042	3.5665	Insignificant
Soft *vs.* Stiff	12.2835	3.5665	Significant
Intermediate *vs.* Stiff	9.5793	3.5665	Significant

Table 4 Tukey's HSD test – front anti-roll bar on gross axle weight rating

Treatments pair	*Tukey HSD Q statistic*	*Tukey HSD Q critical*	*Tukey HSD inference*
Soft *vs.* Intermediate	5.9673	3.5665	Significant
Soft *vs.* Stiff	10.5688	3.5665	Significant
Intermediate *vs.* Stiff	4.6015	3.5665	Significant

3.2 Rear anti-roll bar results

Table 5 presents the maximum absolute fatigue damage values observed on each test configuration for the rear anti-roll bar.

Figure 15 presents a relative fatigue damage analysis of the averaged results from the eight load cases of Table 5. Similar to Figure 14, the results of the intermediate dampers are set as the baseline (100%), while the results from the soft and stiff dampers settings are presented as a percentage of it.

Table 5 Maximum absolute fatigue damage values on the rear anti-roll bar

		Absolute fatigue damage		
Bus weight	*Load case*	*Soft dampers setting*	*Intermediate dampers setting*	*Stiff dampers setting*
CW	1	9.790E-05	8.330E-05	5.390E-05
	2	9.180E-05	8.320E-05	5.240E-05
	3	9.970E-05	9.300E-05	5.230E-05
	4	9.610E-05	9.550E-05	5.400E-05
	5	9.730E-05	9.930E-05	5.590E-05
	6	9.400E-05	1.030E-04	5.370E-05
	7	1.040E-04	1.010E-04	5.080E-05
	8	9.810E-05	1.050E-04	5.230E-05
GAWR	1	1.540E-04	1.220E-04	7.470E-05
	2	1.450E-04	1.090E-04	7.120E-05
	3	1.590E-04	1.230E-04	7.590E-05
	4	1.440E-04	1.100E-04	7.200E-05
	5	1.690E-04	1.290E-04	8.730E-05
	6	1.650E-04	1.300E-04	8.640E-05
	7	1.670E-04	1.300E-04	8.450E-05
	8	1.660E-04	1.320E-04	8.600E-05

Figure 15 Relative fatigue damage analysis of rear anti-roll bar – soft and stiff dampers as a percentage of intermediate dampers setting

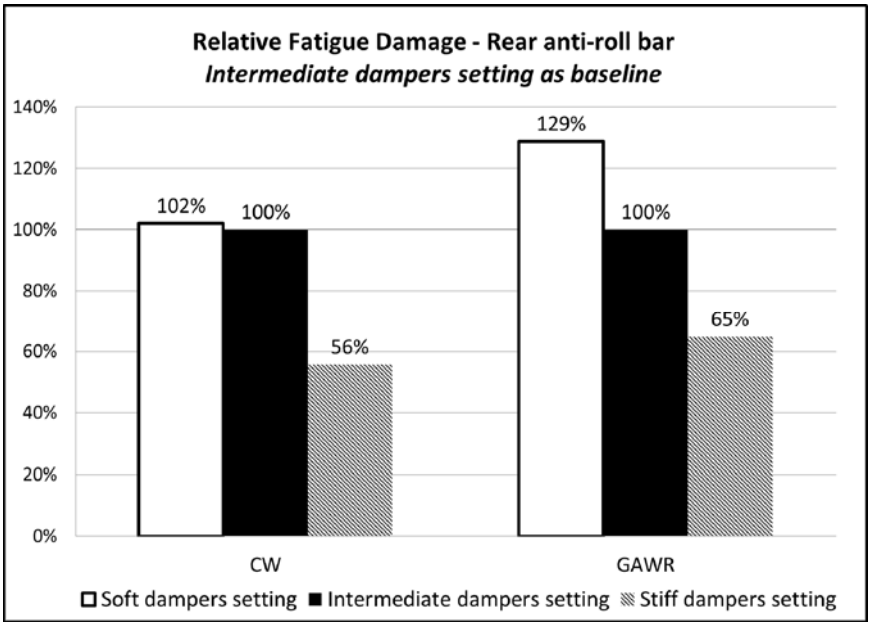

With a statistical significance identified for both curb weight and GAWR configurations, the Tables 6 and 7 present the results of the performed post-hoc Tukey HSD on the data.

Table 6 Tukey's HSD test – rear anti-roll bar on curb weight

Treatments pair	*Tukey HSD Q statistic*	*Tukey HSD Q critical*	*Tukey HSD inference*
Soft vs. Intermediate	1.0247	3.5665	Insignificant
Soft vs. Stiff	23.2267	3.5665	Significant
Intermediate vs. Stiff	22.2020	3.5665	Significant

Table 7 Tukey's HSD test – rear anti-roll bar on gross axle weight rating

Treatments pair	*Tukey HSD Q statistic*	*Tukey HSD Q critical*	*Tukey HSD inference*
Soft vs. Intermediate	11.4637	3.5665	Significant
Soft vs. Stiff	25.4703	3.5665	Significant
Intermediate vs. Stiff	14.0066	3.5665	Significant

Similar to what has been observed on the front anti-roll bar, significant differences have been observed between all analysed pairs, except for the results between the soft and intermediate dampers settings on curb weight.

3.3 Overall results for front and rear anti-roll bar

The results from both front and rear suspension validated the initial hypothesis that different damping rates of shock absorbers can impact the fatigue endurance of anti-roll bars of a commercial vehicle.

The same pattern has been observed in all tested conditions: the higher the damping rate of the shock absorbers, the lower the accumulated damage on the stabiliser bars.

The relative fatigue damage analyses suggested that, in some cases, a softer damper could reduce by almost half the fatigue life of an anti-roll bar when compared to the same bar with stiffer dampers (Figure 15).

However, no statistical significance has been observed between the soft and intermediate dampers settings in the curb weight configuration – for both front and rear suspension. This divergence was further analysed by comparing the velocity levels of the shock absorbers at these two load conditions. In this regard, the time-series data from the string potentiometers (installed on the dampers) were differentiated to obtain the speed. The CW and GAWR configurations were compared for each set of dampers through a level crossing analysis (using nCode Glyphworks™ 13.1), which basically indicates how many times a certain velocity has been crossed. This counting method is based on the theory of rainflow cycle counting (Endo and Matsushi, 1968), where for every instant that the time series signal (in this case the dampers' velocity) crosses a certain limit, a count is performed.

Figure 16 and 17 present the level crossing histograms based on the data of the front stiff and rear soft dampers settings, respectively.

Figure 16 Level crossing histogram of front right stiff dampers – CW and GAWR

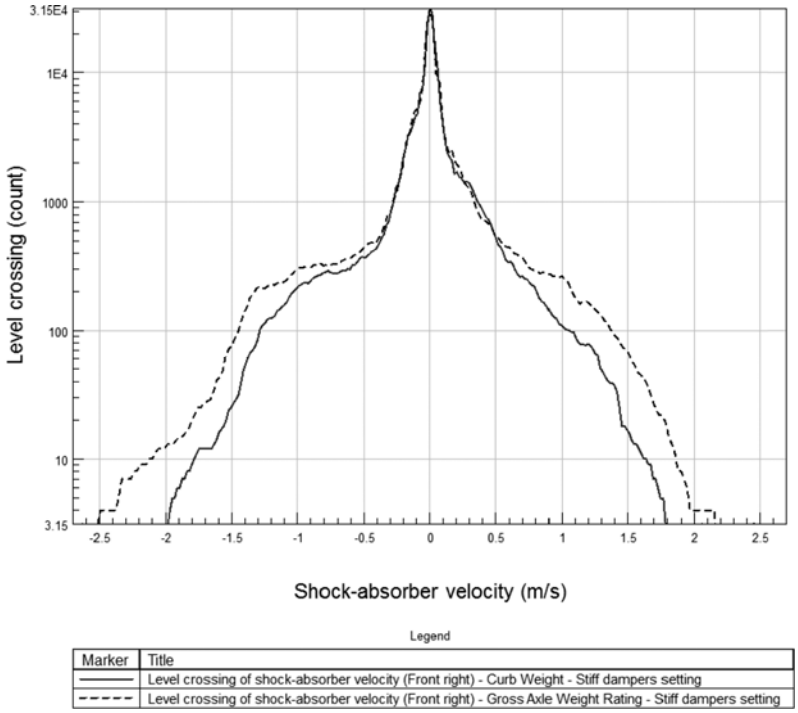

Figure 17 Level crossing histogram of rear left soft dampers – CW and GAWR

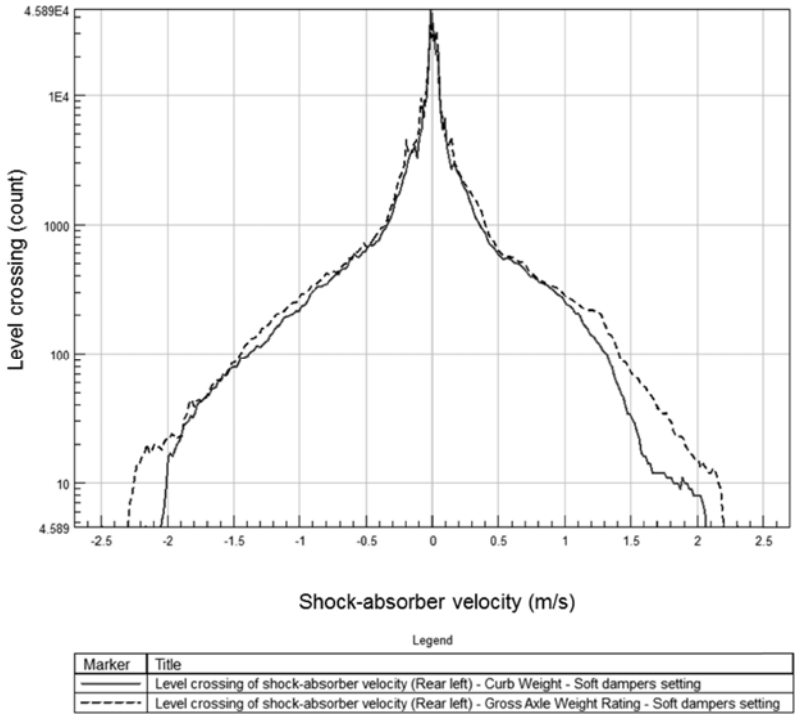

As can be noted from the histograms above, the shock absorbers reached higher peaks of velocity and presented a higher crossing count in upper speeds when tested in GAWR. At lower speeds, CW and GAWR presented very similar results. Although not presented in this work, these results could be confirmed for all shock absorbers settings (soft, intermediate and stiff) and for all positions (front left, front right, rear left and rear front).

As shown in Figures 16 and 17, lower speeds are observed in the shock absorbers during CW testing. Back to Figures 9 and 10, it is possible to note that the damping forces of the soft dampers are similar to the ones from the intermediate settings at lower speeds, in other words, the damping coefficients of the soft and intermediate settings are noted to be closer to each other at those slower speeds. Hence, all this could explain why significant difference between soft and intermediate dampers has been only observed in GAWR configurations.

4 Conclusions

Within the framework of an integrated product development, this study addressed the importance of understanding how different concepts can impact the real loads applied on a given system. It also provides more insight on good testing practices, product optimisation and eventually interim solutions to tackle quality issues in the field.

Based on the theory of fatigue damage accumulation, the durability of the anti-roll bars of a commercial vehicle (front and rear suspension) was assessed for three different shock absorbers' damping rates.

The results from both front and rear suspension suggested that different damping rates of shock absorbers can impact the fatigue endurance of anti-roll bars of a bus. Statistical significance of damage accumulation between different shock absorbers has been identified for both bars on all loading conditions (curb weight and GAWR). The results pointed out that the higher the damping rate was, the lower the detected damage on the stabiliser bars. They also showed that, in some cases, a softer damper could reduce by almost half the fatigue life of an anti-roll bar when compared to the same bar with stiffer dampers.

Further studies are recommended to assess ride comfort characteristics, the impacts of the damping rate on suspended components (such as the vehicle frame) and also to confirm the findings of this work over the usage condition (wear) of the shock absorbers and over a larger sample of commercial vehicles.

Nevertheless, the obtained results are sufficient to highlight the fact that ride comfort and handling tunings should be front-loaded as much as possible during product development. Endurance testing of suspension or complete vehicle should be done after the selection of the shock absorbers. A critical judgement will be needed to delimitate the testing configurations for functional testing prior to the final suspension setting – for some cases the suggestion would be to assess different set-ups and provide the results based on a envelope of data (between most critical to less critical).

References

Abdi, H. and Williams, L.J. (2010) 'Tukey's honestly significant difference (HSD) test', *Encyclopedia of Research Design*, Vol. 1, pp.1–5.

Dixon, J.C. (2007) *The Shock Absorber Handbook*, 2nd ed., Professional Engineering Publishing and John Wiley & Sons, London.

Dowling, N.E. (2012) *Mechanical Behavior of Materials: Engineering Method for Deformation, Fracture and Fatigue*, Pearson, New-Jersey.

Ebrahimi, S.M. (2011) *Concurrent Engineering Approaches within Product Development Processes for Managing Production Start-up Phase*, Unpublished PhD thesis, Tekniska Högskolan, Jönköping, Sweden.

Endo, T. and Matsushi, M. (1968) *Fatigue of Metals Subjected on Varying Stress*, Japan Society of Mechanical Engineers, Fukuoka.

Eriksson, P. and Friberg, O. (2000) 'Ride comfort optimization of a city bus', *Journal Structural and Multidisciplinary Optimization*, Vol. 20, No. 1, pp.67–75.

Eriksson, P. and Friberg, O. (2001) *A Ride Comfort Design Sensitivity Analysis of a City Bus*, SAE Technical Paper 2001-01-2797, DOI: https://doi.org/10.4271/2001-01-2797.

Hambali, A., Sapuan S.M., Ismail, N., Nukman, Y. and Abdul Karim, M.S. (2009) 'The important role of concurrent engineering in product development process', *Pertanika Journal Science & Technology*, Vol. 17, No. 1, pp.9–20.

Harter, H. (1960) 'Tables of range and studentized range', *The Annals of Mathematical Statistics*, Vol. 31, No. 4, pp.1122–1147.

Hassaan, G.A. (2014) 'Car dynamics using quarter model and passive suspension, Part 1: Effect of suspension damping and car speed', *International Journal of Computer Techniques*, Vol. 1, No. 2, pp.19–27.

Haug, E.J. (2012) *Concurrent Engineering: Tools and Technologies for Mechanical System Design*, Springer-Verlag Berlin Heidelberg, Berlin.

Hegazy, S. and Sandu, C. (2009) *Vehicle Ride Comfort and Stability Performance Evaluation*, SAE Technical Paper 2009-01-2859, DOI: https://doi.org/10.4271/2009-01-2859.

Hijawi, M. and Czaja, I. (2004) *Automotive Stabilizer Bar System Design and Reliability*, SAE Technical Paper 2004-01-15, DOI: https://doi.org/10.4271/2004-01-1550.

Jazar, R.N. (2008) *Vehicle Dynamics: Theory and Applications*, Springer Science+Business Media, New York.

Klinikowski, D.J., El-Gindy, M. and Tallon, R.A. (1998) *An Overview of the Federal Transit Administration's Bus Testing Program*, SAE Technical Paper 982774, DOI: https://doi.org/10.4271/982774.

Kokane, G., Nizar, A. and Ravindra, K. (2015) *A Shock Absorber Design with Position Sensitive Damper and Its Performance Evaluation*, SAE Technical Paper 2015-32-0785.

Kubo, P., Paiva C., Ferreira A. and Larocca A. (2015) 'Influence of shock absorber condition on pavement fatigue using relative damage concept', *Journal of Traffic and Transportation Engineering*, Vol. 2 No. 6, pp.406–413.

Liou, H.Y., Wu, W. and Shin, C. (1999) 'Modified model for the estimation of fatigue life derived from random vibration theory', *Probabilistic Engineering Mechanics*, Vol. 14 No. 3, pp.281–288.

McNaull, P.J., Salaani, M.K., Guenther, D.A., Grygier, P.A. and Heydinger, G.J. (2010) 'Integration of a torsional stiffness model into an existing heavy truck vehicle dynamics model', *SAE International*, Vol. 3, No. 1, pp.175–186.

Milburn, T.J. (2004) *The New Product Development Paradigm Led by Simulation and Testing*, SAE Technical Paper 2004-01-2667, DOI: https://doi.org/10.4271/2004-01-2667.

Miner, M.A. (1945) 'Cumulative damage in fatigue', *Journal of Applied Mechanics*, Vol. 12, No. 3, pp.159–164.

Neal, M.W., Cwycyshyn, W. and Badiru, I. (2015) 'Tuning dampers for ride and handling of production vehicles', *SAE International*, Vol. 8, No. 1, pp.152–159.

Noraishikin, Z., Fitrian I., Zamzuri, H. and Mazlan S. A. (2012) 'Application of an active anti-roll bar system for enhancing vehicle ride and handling', Paper Presented at the *2012 IEEE Colloquium on Humanities, Science and Engineering (CHUSER)*, Kota Kinabalu, Malaysia, pp.260–265.

Rakheja, S., Ahmed, A.K.W., Yang, X. and Guerette, C. (1999) *Optimal Suspension Damping for Improved Driver-and Road-Friendliness of Urban Buses*, SAE Technical Paper 1999-01-3728, DOI: https://doi.org/10.4271/1999-01-3728.

Rana, J., Gajjar, S. and Pate, I.A. (2014) 'Experimental analysis and heat transfer study of damping fluid in shock absorber operation', *International Journal of Engineering Development and Research*, Vol. 2, No. 3, pp.2939–2946.

Ribeiro, S.Y. and Silveira, M.E. (2013) *Application of Finite Element Method in the Study of Variables that Influence the Stiffness of the Anti-Roll Bar and the Body Roll*, SAE Technical Paper 2013-36-0643, DOI: https://doi.org/10.4271/2013-36-0643.

Sapuan, S.M., Osman, M.R. and Nukman Y. (2006) 'State of the art of the concurrent engineering technique in the automotive industry', *Journal of Engineering Design*, Vol. 17 No. 2, pp.143–157.

Senapathi, P., Shamasundar, S., Venugopala, R.G. and Sachin, B.M. (2009) *Endurance Testing and FE Analysis of Four Wheeler Automobile Stabilizer Bar*, SAE Technical Paper 2009-26-0066, DOI: https://doi.org/10.4271/2009-26-0066.

Sert, E. and Pinar, B. (2017) 'Optimization of suspension system and sensitivity analysis for improvement of stability in a midsize heavy vehicle', *Elsevier*, Vol. 20, No. 3, pp.997–1012.

Soone, R.G., Gummadi, L.N.B. and Cao, K.D. (2005) *Robustness Considerations in the Design of a Stabilizer Bar System*, SAE Technical Paper 2005-01-1718, DOI: https://doi.org/10.4271/2005-01-1718.

Su, H. (2014) *A Road Load Data Processing Technique for Durability Optimization of Automotive Products*, SAE Technical Paper 2014-01-0884, DOI: https://doi.org/10.4271/2014-01-0884.

Tan, C.L. and Vonderembse, M. (2006) 'Mediating effects of computer-aided design usage: from concurrent engineering to product development performance', *Journal of Operations Management*, Vol. 24, No. 5, pp.494–510.

Topaç, M.M., Enginar, E.H. and Kuralay, N.S. (2011) 'Reduction of stress concentration at the corner bends of the anti-roll bar by using parametric optimisation', *Mathematical and Computational Applications*, Vol. 16, No. 1, pp.148–158.

Zhang, N., Qi, H., Zhang, B. Zheng, M. and Chen, Y. (2019) 'Enhanced Lateral and Roll Stability Study for a Two-Axle Bus via Hydraulically Interconnected Suspension Tuning', *SAE Int. J. Veh. Dyn., Stab., and NVH*, Vol. 3, No. 1, pp.5–18.

Zhu, H., Yang, Y., Yang, Y., Zeng, J. and Zhang, Y. (2014) *Ride Optimization for a Heavy Commercial Vehicle*, SAE Technical Paper 2014-01-0843, DOI: https://doi.org/10.4271/2014-01-0843.

Zhu, S-P., Huang, H-Z. and Wang, Z-L. (2011) 'Fatigue life estimation considering damaging and strengthening of low amplitude loads under different load sequences using fuzzy sets approach', *International Journal of Damage Mechanics*, Vol. 20 No. 6, pp.876–899.